Macromolecules

pubs.acs.org/Macromolecules

Article

Toward *In Silico* Design of Highly Tunable Liquid Crystal Elastomers

Ethan I. L. Jull, Richard J. Mandle, Thomas Raistrick, Zhaopeng Zhang, Peter J. Hine, and Helen F. Gleeson*

Cite This: https://doi.org/10.1021/acs.macromol.2c00587

Read Online

ACCESS | Metrics & More | Article Recommendations | Supporting Information

ABSTRACT: In this work, a two-component acrylate liquid crystal elastomer, with varying composition and templating phase, is synthesized in the laboratory and investigated in parallel using atomistic molecular dynamics simulations. The anisotropic nature of both the mono- and bifunctional acrylates used in this study enables a large tunability in the compositional range while still retaining liquid crystalline properties in the final elastomer. The use of simulations allows important evaluation and comparison of physical properties such as glass transition temperature, nematic to isotropic phase transition temperature, and order parameter. The dependence of physical properties (glass transition, nematic to isotropic transition, order parameter, coefficient of thermal expansion, and mechanical properties) is established as a function of chemical composition, showing a high degree of tunability. Interestingly, the templating phase (nematic or isotropic) is also shown to impact the subsequent elastomer properties, with excellent agreement shown here between experiments and simulations. The *in silico* approach to polymerization, coupled with excellent comparison with the experimental system, represents a new methodology for the targeted design of liquid crystal elastomers with specific physical properties.

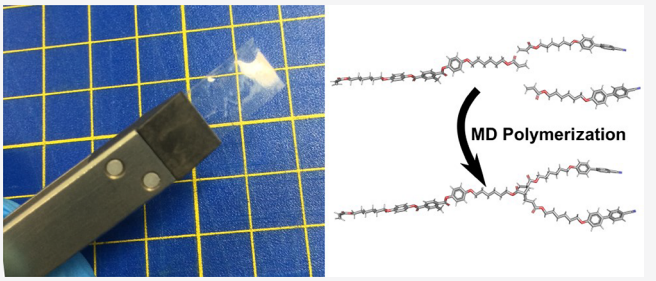

INTRODUCTION

The ability to design materials with specific properties, both experimentally and *in silico*, is crucial for materials application development. Liquid crystal elastomers (LCEs) combine the anisotropic properties of liquid crystals (LCs)[1] with the elasticity of a polymer network.[2] The coupling of nematic order to the polymer backbone results in anisotropy in the polymer random walk and gives a corresponding anisotropic response to external stimuli (e.g., irradiation, heating/cooling, chemical, or electrical).

Many LCE investigations focus on their direct applications such as artificial muscles,[3−5] energy absorption,[6−8] or soft robotics.[9] A growing number of studies have begun to explore the pure mechanical properties of LCEs.[10−12] Such studies typically report on a single chemical composition and single synthesis templating. There is an emerging ability to control properties through chemical composition[13−17] or synthesis templates,[14,18] though the complexity of some LCE fabrication techniques can make modifications in this regard difficult. There is a need for in-depth studies of LCE property dependence on chemical composition and synthetic templates (specifically whether the polymer is templated through synthesis in a nematic or isotropic phase (nLCE or iLCE)). Such in-depth studies will allow for LCE material design with targeted properties for specific application needs.

This paper reports on a model LCE two-component system that has allowed us to explore experimentally the dependence of LCE properties on chemical composition and synthesis templates. Specifically, the synthesis methodology is varied to compare the properties of isotropic and nematic templated LCEs with equivalent chemical composition. The experimental findings are subsequently rationalized *via* novel molecular dynamics (MD) simulations. In MD simulations, we use a heuristic protocol that permits the modeling of acrylate polymerizations in atomistic, fixed-valence MD simulations. The paper is organized as follows: first, LCE synthesis, MD simulation, and characterization techniques are described. The phase diagram of the binary monomer mixture, crucial for LCE synthesis template design, is then explored using predictive methods combined with experimental validation. The LCE thermal properties, glass transition temperature (T_g), order parameter ($\langle P_2 \rangle$), nematic to isotropic transition temperature (T_{NI}), and coefficient of thermal expansion (CTE), are then explored, for both nLCEs and iLCEs, as a function of chemical composition. Thermal properties are investigated through a combination of MD simulation and experimental characterization. Finally, the mechanical properties of the iLCE are characterized experimentally as a function of chemical composition.

Received: March 22, 2022
Revised: May 5, 2022

This report demonstrates a large tunable range in thermal and mechanical properties across the composition parameter space, allowing for targeted material design. The coupling of nematic order to the LCE network is also explored, a crucial characteristic underpinning many LCE properties utilized in applications. Material characterization is undertaken, and the underlying mechanisms behind property dependencies are thoroughly explored, with improved insight enabled through novel LCE MD simulations. LCE property tunability is clearly demonstrated, and the ability to utilize *in silico* design for targeted LCE material synthesis is established for the first time.

MATERIALS AND METHODS

LCE Synthesis. The LCEs studied are composed from binary mesogenic monomer mixtures, with varying amounts of monofunctional acrylate 4-[(6-acryloyloxy)hexyloxy]-4′-cyanobiphenyl (A6OCB, TCI Chemicals) and bifunctional acrylate (crosslinker) 1,4-bis-[4-(6-acryloyloxyhexyloxy)benzoyloxy]-2-methylbenzene (RM82, Merck), shown in Figure 1a. These monomers were selected

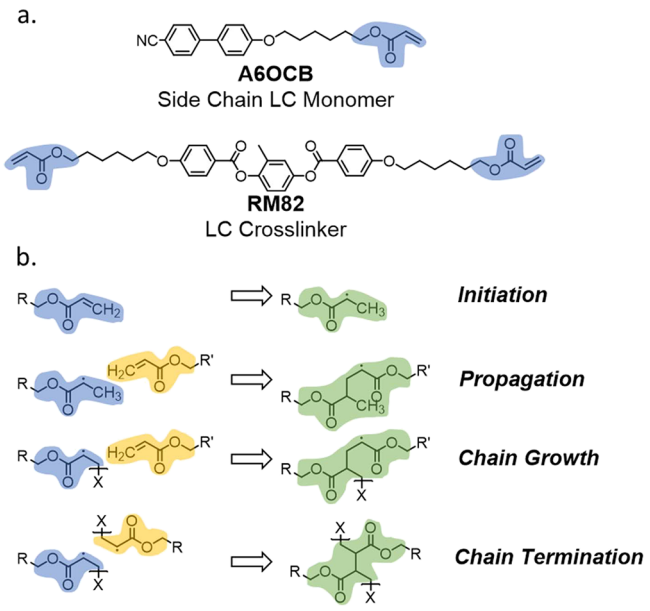

Figure 1. (a) Monofunctional acrylate monomer A6OCB and bifunctional acrylate monomer (crosslinker) RM82 chemical structures are shown. (b) Examples of the four reaction schemes employed during reactive MD for the head-tail reaction between acrylates, and the chemical structures of materials used in simulations with their reactive portion highlighted in blue. A reaction occurs when reactant molecule(s) with topologies as shown in yellow and blue are within the threshold distance (r_{cutoff}), and in the case of initiation, the total number of reactions is below the specified limit. After a bond forms, the force field parameters are updated for the region highlighted in green. R and X are edge atoms and connect to either some side group (R) or the polymer chain (X).

due to their anisotropic nature, each demonstrating an LC nematic phase (Figure 2). The monomer anisotropy allows for a large chemical composition parameter space, much larger than previously explored,[13,15−17] to be investigated without the loss of nematic order in the final LCE sample. LCE samples of varying composition were explored from 0 to 100 mol % RM82, in approximate steps of 10 mol %, where monomer mixture phase transition temperatures were allowed.

Synthesis of well-aligned, homogeneous, LCE samples was achieved *via* photopolymerization of monomer mixtures while being constrained between surface-treated glass and Melinex (Type 401)

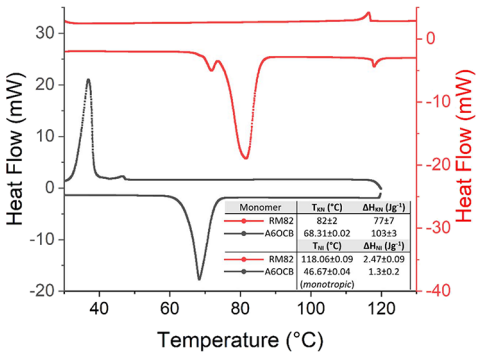

Figure 2. Heat flow versus temperature measured *via* DSC for pure monomers RM82 (red, right-axis, top trace) and A6OCB (black, left-axis, bottom trace). The table inset shows the phase transition temperatures and associated enthalpies.

substrates, separated by 100 μm spacers. Both substrates were treated with an alignment layer to promote in-plane alignment of LC mesogens; the alignment layers were then rubbed with felt and oriented such that planar alignment is achieved in the final mold.

The monomers were mixed at 120 °C, at various ratios, with approximately 1.8 mol % methyl benzoylformate as the photo initiator, to explore the available composition range. The monomer mixture was capillary filled into the mold while in the isotropic phase to avoid flow-alignment that can occur when filling in the nematic phase. For preparation of nLCEs, the sample was cooled to approximately 10 °C below T_{NI} and simultaneously kept at a minimum of 5 °C above the solid/crystal melting point (T_{KN}). For preparation of iLCEs, the sample was kept at least 10 °C above T_{NI}. Samples were held at their respective temperatures for 15 min to ensure that the homogeneous phase formation had evolved. Polymerization was triggered using a 2.5 mWcm^{-2} fluorescent UV light source for 2 h while maintaining constant sample temperature. The polymerized LCE films were then removed from the mold for testing and characterization.

MD Simulation Setup. MD simulations were performed in LAMMPS;[19] parameters for acrylate monomers were modeled using the General Amber Force Field (GAFF).[20] Independent starting configurations were generated using PACKMOL to minimize atomic overlap.[21]

Each simulation contains a total of 500 monomer molecules, A6OCB and/or RM82, in a cubic box with *xyz* periodic boundary conditions. The ratios of A6OCB and RM82 in each simulation were chosen to explore the full chemical composition parameter space. First, energy minimization and equilibration are performed under *NVE* and *NVT* ensembles, respectively, with the latter being at 600 K to ensure the absence of orientational and positional order. A 5 ns compression simulation was run in the *NPT* ensemble using an isotropic barostat with a pressure of 100 bar to yield a liquid-like simulation density. A further equilibration MD simulation was performed in the *NPT* ensemble (T = 300 K or 400 K, P = 1 bar) for up to 100 ns; the 400 K simulation remains isotropic, whereas for the 300 K simulations, nematic order emerges. Production MD runs were then performed under the *NPT* ensemble for each simulation box for 250 ns at a temperature of 300 K (for nematic simulations) or 400 K (for isotropic simulations) and a pressure of 1 atm. We refer to these as pre-reacted simulations.

Although atomistic MD simulations of low molecular weight nematic LCs are well-known, simulation of polymerization within a nematic phase to form an LCE has not been attempted with atomistic detail. We simulated acrylate polymerizations using the REACTER protocol, implemented in LAMMPS as fix bond/react, described by Gissinger *et al.*[22,23] Briefly, REACTER is a proximity-based scheme that scans the simulation for eligible reactive sites, the topologies of which are described in a pre-reaction template. After a bond is formed, the local force field topology (atom, bond, angle, dihedral, and improper types) is updated according to a post-reaction template

https://doi.org/10.1021/acs.macromol.2c00587
Macromolecules XXXX, XXX, XXX−XXX

that reflects the new chemical identity of the reacted species. Figure 1a shows the two acrylate monomers (A6OCB and RM82) used in our simulations, with the reactive portion highlighted in blue. Figure 1b shows the four reactions defined for head-tail reactions; color coding shows which regions undergo changes to topology during each reaction (blue and yellow) and the resulting new topology (green). R and X are edge atoms and connect to either a side-group (R) or the polymer chain (X); in the case of X, additional atoms are defined in the pre- and post-reaction template, which are omitted from Figure 1b for clarity. The defined reactions between a radical species and acrylate can only occur when the reactants are within a cut off distance (r_{cutoff}) of 3.5 Å; over the course of the polymerization, r_{cutoff} is gradually increased to a maximum of 5 Å to ensure that a high degree of polymerization is achieved within a reasonable simulation time. We refer to these as polymerization simulations.

All polymerization simulation trajectories were performed in the *NPT* ensemble with a time step of 0.5 fs at a pressure of 0.1 MPa and a temperature of either 300 K (nematic) or 400 K (isotropic). The choice of temperature is to ensure the presence (or absence) of orientational order throughout the polymerization process. The number of initiation reactions was limited to mimic the experimental initiator concentration of ∼1.8 mol %, which corresponds to nine discrete initiations, defined in Figure 1b. The reaction portion of each simulation trajectory was run for 30 ns in total. The percentage conversion was obtained from the cumulative reaction counts and the number of acrylate units present pre-reaction.

For nematic MD simulations a further 250 ns simulation was then performed in the *NPT* ensemble with a time step of 0.5 fs, a pressure of 1 atm, and a temperature of 300 K; for all trajectory frames recorded during this production MD run, we calculated the orientational order parameter $\langle P_2 \rangle$ (as described in the MD Post-simulation Analysis Section below). We refer to these as post-reacted simulations.

MD Post-simulation Analysis. T_g is obtained from MD simulations by conducting a temperature ramp from 500 to 200 K, recording the density of the simulation. The T_g of a given simulation is located by finding the intercept between two linear fits to the density: one for temperatures 15 K or more below T_g and one for temperatures 15 K or more above T_g.

The second-rank orientational order parameter, $\langle P_2 \rangle$, is calculated *via* the *Q*-tensor approach according to eq 1

$$Q_{\alpha\beta} = \frac{1}{N}\sum_{m=1}^{N}\frac{3\alpha_{m\alpha} - \delta_{\alpha\beta}}{2} \tag{1}$$

where N is the number of LC moieties (e.g., RM82 and/or A6OCB; 500 in all simulations), m is the monomer number within a given simulation, α and β indicate two Cartesian directions, and θ_α and θ_β are the angles between the inertia axis of a given monomer unit and the α and β directions, respectively. The angled brackets indicate that an ensemble average is taken for all molecules at a given time step. The order parameter $\langle P_2 \rangle$ corresponds to the largest eigenvalue of $Q_{\alpha\beta}$. Order parameter calculations, director mapping, and densities were computed using MDTraj.[24] MD trajectories were visualized with VMD.[25]

Experimental Characterization Methods. Differential scanning calorimetry (DSC)[26] of the materials was conducted using a TA Q-20 DSC to identify the phase transitions, T_{NI}, and T_{KN}, in the monomer mixtures. DSC was also employed to measure T_g in the final polymerized LCE samples; however, the LCE T_{NI} remained undetectable at temperatures below thermal degradation. For unpolymerized monomer mixtures, the samples were heated and cooled at 10 °Cmin^{-1} between a minimum of −30 °C and maximum of 135 °C (avoiding monomer mixture T_g and thermal polymerization, respectively) with 30 min isothermal time to allow crystallization to occur. For polymerized LCEs, the sample was heated and cooled at 10 °Cmin^{-1} between a minimum of −30 °C and a maximum of 200 °C.

The CTE was measured through imaging of a sample cut to approximately 1 × 2 cm using a Nikon D7100 while on a UniTemp GmbH HP-220 hotplate allowing the macroscopic shape of the LCE sample to be measured as a function of temperature from 30 to 200 °C. The LCE had little to no adhesion to the hot plate surface and therefore had free movement to allow for expansion and contraction to be accurately monitored.

Dynamic mechanical analysis (DMA) was performed using a Rheometrics Solid Analyzer II. Samples of iLCE were cut into nominal dimensions of 5.5 × 2 × 0.1 mm and then were placed under tension at 0.1 N. Single frequency measurements were performed at 1 Hz with a strain of 0.1%. The storage modulus (E'), loss modulus (E''), and tan(δ) were recorded, and repeats were conducted on each sample (with multiple samples of identical composition cut) to confirm repeatability. Since each specific composition polymer has a different T_g, the dynamic mechanical behavior was determined at 30 °C above the T_g identified by DSC. A full temperature scan was performed at 1 Hz on samples with 39.2 mol % and 78.4 mol % RM82 to determine the thermal behavior of the single frequency measurements taken above T_g.

The order parameter was determined experimentally *via* polarized Raman spectroscopy using the Raman depolarization ratio method.[27,28] The Raman spectra were collected using a Renishaw inVia confocal Raman microscope in a reflection geometry. A 532 nm solid-state laser was focused onto the sample using a 50× objective, with the laser power controlled *via* a notch filter. The Raman signal was captured *via* an integrated CCD and analyzed using WiRE data acquisition software. For temperature-dependent measurements, a Linkam TMS93 hotstage was used to control the temperature of the sample with a relative accuracy of ±0.1 °C. A rotation stage enabled the spectra to be collected as a function of the angle between the laser polarization and the sample director. For room temperature measurements, a full rotation of 360° was used with 10° increments. Temperature-dependent measurements were restricted to 180° rotation at 10° intervals by the hotstage. To deduce the order parameter of the system the Raman active phenyl stretching mode at 1606 cm^{-1} was used for analysis, with further details in references 27, 28.

RESULTS AND DISCUSSION

Monomer Mixture Phase Diagram. Fabrication of a homogeneous nLCE film, *via* monomer polymerization in a surface-aligned mold, relies on polymerization of the monomer mixture in the nematic phase. It is of critical importance to avoid recrystallization during polymerization, and therefore the T_{KN} of the monomer mixture is of equal importance to the T_{NI}. The ability to theoretically predict monomer mixture phase transition temperatures enables ease of synthesis template design, removing the need for time-consuming mixture phase diagram mapping. For a multi-component system, such as the monomer mixture utilized in this study, the phase transition temperatures can be approximated by the Schröeder-van-Laar equation:

$$\ln \chi_A = \frac{\Delta H_A\left(\frac{1}{T_A} - \frac{1}{T}\right)}{R} \tag{2}$$

where ΔH_A is the enthalpy of fusion of pure component A, T_A is the phase transition temperature of pure component A, T is the phase transition temperature of the mixture containing the mole fraction χ_α, and R is the gas constant.[29,30] To utilize eq 2 for the prediction of the phase transition temperatures of the LCE monomer mixtures, the transition temperatures and associated enthalpies of fusion of the pure monomer components RM82 and A6OCB must be established. Figure 2 demonstrates the heat flow as a function of temperature measured *via* DSC for RM82 and A6OCB, with the inset

https://doi.org/10.1021/acs.macromol.2c00587
Macromolecules XXXX, XXX, XXX−XXX

summarizing the resulting phase transition temperatures and enthalpies.

The phase transition temperatures of the unpolymerized monomer mixtures were determined *via* DSC with varying RM82 molar concentrations from 0 to 100 mol %, in approximately 10 mol % steps, and compared to the predicted values in Figure 3. We find the experimentally determined values of T_{KN} and T_{NI} to be in good agreement with predictions made with the Schröeder-van-Laar equation. The nematic phase becomes monotropic for monomer mixtures with less than 25 mol % RM82, and therefore, fabrication of homogeneous nLCE samples at concentrations <25 mol % is difficult due to recrystallization disrupting alignment.

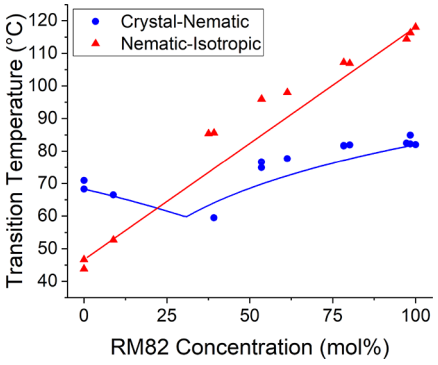

Figure 3. The monomer mixture phase transition temperatures as a function of RM82 molar concentration are shown. The solid lines are the Schröeder-van-Laar predictions calculated utilizing pure monomer component phase transitions and associated enthalpies (Figure 2, eq 2). Experimental data, measured *via* DSC, demonstrate good agreement with predictions.

Figure 3, and by extension of the Schröeder-van-Laar equation, can be utilized in the synthesis template design by determining temperatures at which the photopolymerization should be conducted for generation of either well-aligned nLCE films or homogeneous iLCE films (as described in the Materials and Methods Section). With the binary monomer mixture phase diagram accurately mapped, the fabrication of homogeneous LCE films can take place and the analysis of their properties' dependence on composition or the phase in which the polymerization took place can be experimentally determined.

LCE Glass Transition Temperature (T_g). The mechanical, energy absorbing, and thermal coefficient properties of polymers all vary as a function of temperature, especially around the glass transition.[12] Therefore, the T_g of an LCE is a crucial design consideration in development of LCE materials for applications. We now explore the dependence of T_g on crosslinker (RM82) concentration and the templating phase in which the LCE is polymerized (nematic or isotropic) for the A6OCB/RM82 system using both experimental (DSC) and computational (MD simulations) approaches. This combined approach enables us to investigate the dependency and underlying mechanisms involved while simultaneously demonstrating the ability for the MD predictive approach to be utilized in the design of LCEs with a pre-defined glass transition.

T_g Composition Dependence. Samples of iLCE were fabricated with RM82 concentrations varying from 0 to 80 mol % RM82; concentrations at >80 mol % RM82 were unable to generate homogeneous isotropic films. While thin-film samples of 0 mol % RM82 (100 mol % A6OCB) LCE could not be made due to the lack of crosslinker, the T_g of a "bulk" sample, polymerized in the isotropic phase, could still be determined. The measured T_g for iLCEs as a function of composition,

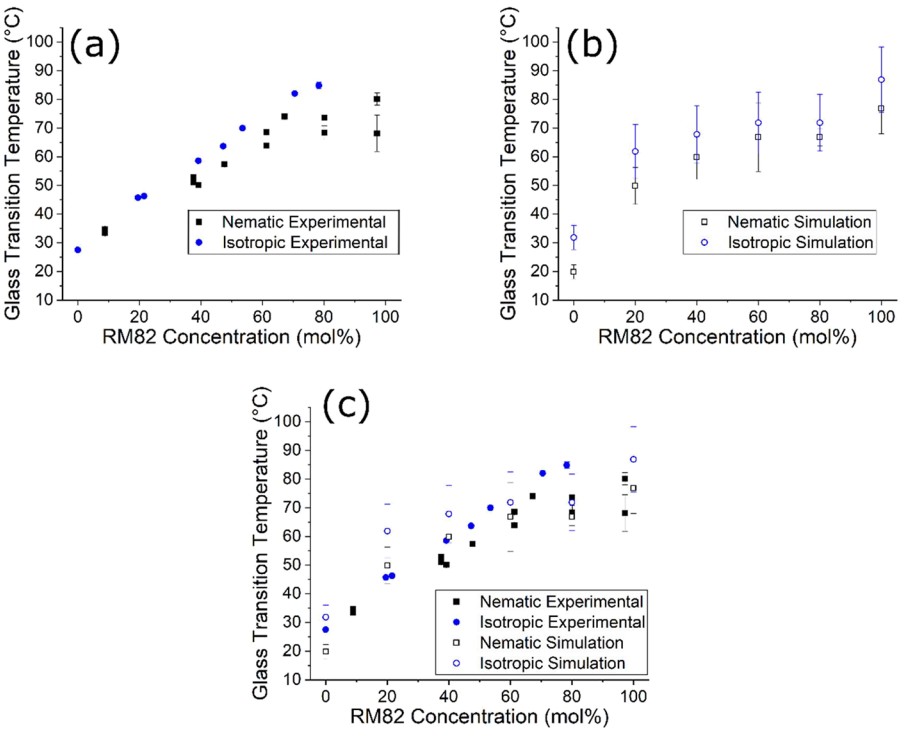

Figure 4. Glass transition temperature measured *via* (a) DSC and (b) MD simulations as a function of RM82 molar concentration for iLCEs and nLCEs. (c) Direct comparison between experimental and simulation results.

https://doi.org/10.1021/acs.macromol.2c00587
Macromolecules XXXX, XXX, XXX−XXX

determined *via* DSC, is summarized in Figure 4a. Increasing the concentration of the RM82 crosslinker from 0 to 80 mol % in iLCEs generates an approximately linear increase in T_g from 27.5 to 84.8 °C.

Samples of nLCE were fabricated with RM82 concentrations varying from 10 to 100 mol % RM82. At concentrations of <25 mol % RM82, the fabrication of a well-aligned nematic LCE is difficult due to the monotropic nature of the nematic phase for these monomer mixtures (Figure 3), with the resulting samples having typically poor alignment compared with the higher-concentration RM82 LCEs. The measured T_g for nLCEs as a function of composition is also summarized in Figure 4a. Increasing the concentration of the RM82 crosslinker from 10 to 100 mol % generates an approximately linear increase in T_g from 33.4 to 80.1 °C, with a hint at a plateau region at concentrations above 70 mol %. It is noted that the nLCE T_{NI} was not observed *via* DSC within the measurable range.

Samples of iLCE and nLCE were simulated from 0 to 100 mol % RM82, in steps of 10 mol %, as described in the Materials and Methods Section. Figure 4b demonstrates T_g as a function of RM82 concentration determined for the MD simulated LCE systems, demonstrating good agreement with experimental results (Figure 4c).

The observed increases in T_g in both the iLCE and nLCE samples are a direct result of increasing the crosslinker density in the sample, which in turn restricts the segmental chain relaxations responsible for the glass transition. This agrees with previous studies exploring the impact of crosslinker density on the T_g of LCEs, though the tunable range in T_g demonstrated here is much larger than any previously reported for LCE materials.[13,15−17,31] The ability to tune T_g to such a large extent is a direct result of the mesogenic nature of both monomer components of this system. Whereas other fabrication techniques typically explore a smaller crosslinker variable space, the use of a mesogenic tri-functional crosslinker demonstrates an impressive range in T_g (T_g varies 38.3−70.6 °C with 4.7−47.2 mol % tri-functional crosslinker range).[31] The crosslinker variable space to explore is due to the techniques involving the non-mesogenic crosslinker concentration (T_g varies 26−34 °C with 5−15 mol % crosslinker range)[16] or non-mesogenic spacer ratio control (T_g varies 4.1−16 °C with 0.9−0.5 mol ratio spacer: diacrylate).[13,17] Thiol-acrylate Michael-addition techniques also have similar restrictions in which the thiol-monomer/spacer/crosslinker is non-mesogenic and thus the ratio of thiol to diacrylate can only be varied over a restricted range (T_g varies 3.7−18.2 °C with 4.7−23.3 mol % crosslinker range).[15] The crosslinker concentration parameter space is smaller for these previously reported systems as increasing the non-mesogenic component concentration reduces the monomer mixture nematic temperature range and thus prevents fabrication of nLCE samples. However, the nematic nature of both monomer components in the system utilized here allows for a large range of crosslinker concentrations and therefore a much larger tunability in T_g.

T_g Templating Dependence. Interestingly, the experimental iLCE samples have a systematically elevated T_g when compared to nLCEs with equivalent RM82 concentrations (Figure 4a). Across the comparable concentration range (10 to 80 mol % RM82), there is approximately an increase in T_g of (9 ± 2) °C when comparing iLCEs to nLCEs. To explore this further, we turn to MD simulations.

T_g measured *via* MD simulation also exhibits a near identical elevation in T_g for iLCEs compared to nLCEs of the identical composition, with an average increase across the concentrations of (9 ± 1) °C. We can utilize the MD simulations as a "computational microscope" to probe the underlying mechanism involved in this increase in T_g observed for iLCEs, something more difficult in purely experimental studies.

All simulations feature regions that are relatively rich in unreacted monomers, these being trapped far from reactive sites of the growing polymer network by the network itself. Nevertheless, all simulations achieved high degrees of conversion; in all cases, the resulting polymer chains repeatedly cross the periodic boundary giving, in effect, an infinitely long network/chain. For simulations including the bifunctional acrylate RM82, the backbones are also crosslinked. Figure 5 presents the images of a typical nematic post-reaction simulation.

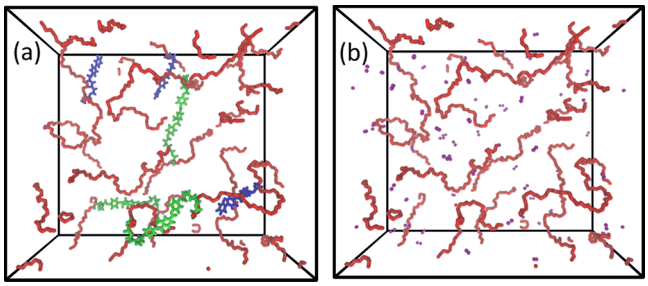

Figure 5. Snapshots of a typical post-reaction nematic simulation (80 mol % A6OCB and 20 mol % RM82). In both images, the polymer backbone is presented as a red tube: (a) shows three monomers each of A6OCB (blue) and RM82 (green), randomly selected, which form part of the polymer network; (b) shows the locations of unreacted acrylate C═C atoms (purple) following completion of the polymerization simulation. We elect to visualize just a few side-groups to enable the entirety of the polymer network to be seen unobscured. In both images, the blue box is the periodic simulation boundary.

The degree of polymerization (p%) was calculated by dividing the number of reacted acrylates by the initial number in each simulation. Figure 6a shows the p% as a function of RM82 concentration and phase templating type, with T_g results included for ease of comparison. In isotropic simulations, a high degree of conversion is obtained, with all simulations being >95% polymerized, whereas the conversion is ∼87% in the nematic phase. At any given RM82 concentration, the degree of polymerization is around 10% lower in the nematic simulation than in the corresponding isotropic simulation.

This increase in p% for isotropic systems compared to their nematic counterparts is most likely a consequence of the reduced diffusion of unreacted monomers within the nematic system when compared to the isotropic case.[32] As noted above, pockets of unreacted monomers can be trapped by the growing polymer network in both simulations; however, in the nematic case, the reduced diffusion means that these monomers are less likely to move proximal to a reactive site and partake in a chain growth reaction than for isotropic systems. Park and Kamal[33] used FT-IR measurements to show that the diacrylate crosslinker RM257 (homologous in structure to RM82) saturates at 76% conversion when polymerized in the nematic phase. With this reassurance that the degree of conversion seen in our MD simulations corresponds with experimental reality, the impact of this conversion on T_g is now established.

https://doi.org/10.1021/acs.macromol.2c00587
Macromolecules XXXX, XXX, XXX−XXX

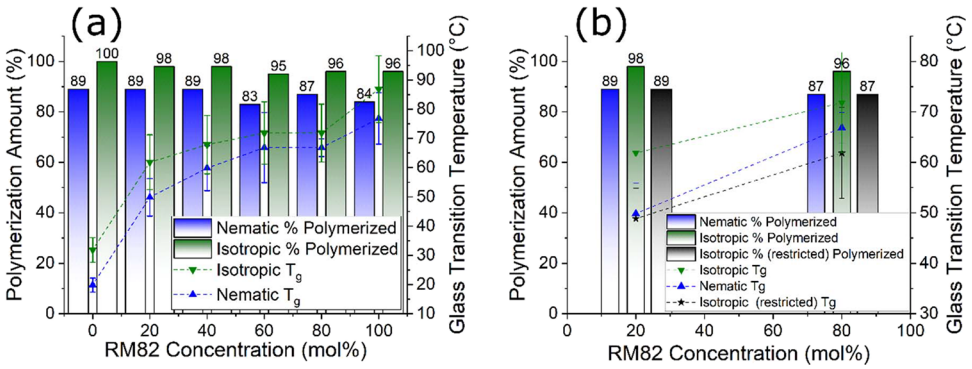

Figure 6. (a) The degree of polymerization is plotted as a function of RM82 concentration (0−100 mol % in 20 mol % increments) for nematic and isotropic LCEs. The associated glass transition for each concentration/phase is also shown. (b) Percentage polymerization plotted for the nLCE together with restricted and non-restricted iLCE for 20 and 80 mol % RM82. The associated glass transition for each is also shown.

To ensure that a higher conversion in iLCE is the underlying cause of the higher T_g compared to the nLCE, the MD simulation for the 20 and 80 mol % RM82 systems was repeated for the isotropic templating; however, this time with the p% restricted to match that of their nematic counterparts. Moreover, the maximum number of each specific reaction (Figure 1) that could take place was restricted to replicate those that occur in the nematic polymerization simulation. Figure 6b demonstrates the comparison of the restricted and non-restricted iLCE with their nematic counterparts. A reduction in T_g is observed for the restricted-isotropic LCEs to temperatures within 5 °C of their unrestricted-nematic LCE counterparts, indicating that it is the conversion percentage that is responsible for the elevated T_g observed in iLCEs compared to the nLCEs here.

There are few experimental comparable investigations of the impact of LCE polymerization state (isotropic or nematic) on T_g to which the results presented here can be compared. Traugutt *et al.*[14] investigated the impact of synthesis phase on a thiol-acrylate main chain LCE system by conducting the thiol-acrylate addition in solvent (isotropic) or at elevated temperatures (nematic). Both methods resulted in a polydomain nLCEs, unlike the LCEs reported here. The difference in polymer synthesis, chemistry, and final LCE state is important to note; however, Traugutt *et al.* did report an elevated T_g for isotropic-synthesis route LCEs compared to their nematic counterparts. It is possible to draw similar conclusions surrounding polymerization conversion percentages. The LCE samples fabricated in solvent by Traugutt *et al.* will have had an increased monomer mobility and thus may have an increased overall conversion, thus generating their reported elevation in T_g.

Figure 6a also demonstrates a gradual reduction in the total conversion in the simulations with increasing RM82 concentration. This may also help explain why the T_g appears to plateau at high RM82 concentrations in MD simulation results, with hints of plateauing for high concentration nLCEs in experimental results (Figure 4). This is likely a direct result of a reduced mobility of the larger RM82 monomer material when compared with the A6OCB monomer, and therefore, the conversion drops and results in the increase in T_g, being no longer directly proportional to the molar concentration of RM82 (number of crosslinks) as there is no full conversion of the RM82 population.

LCE Order Parameter. The order parameter, $\langle P_2 \rangle$, of LCEs is a crucial characteristic to quantify in the design of LCEs for application. Due to the coupling between backbone anisotropy and the nematic order parameter, the temperature dependence of the order parameter is especially important for LCEs where a spontaneous shape change, in response to external stimuli, is desired. We first explore the dependence of $\langle P_2 \rangle$ on composition for the nLCE systems at room temperature before probing the temperature dependence of the varying compositions using both experimental (Raman spectroscopy) and computational (MD simulation) approaches.

Post-polymerization $\langle P_2 \rangle$ Composition Dependence. $\langle P_2 \rangle$ was measured at room temperature *via* Raman spectroscopy on monodomain nLCE samples, with results summarized in Figure 7. Measurements on nematic samples with concentrations <25 mol % RM82 was not possible due to monomer mixture phase transition temperatures as discussed in previous sections. The nLCE system demonstrates a near constant order parameter as a function of composition, with an average $\langle P_2 \rangle$ of (0.61 ± 0.02) across the measured samples.

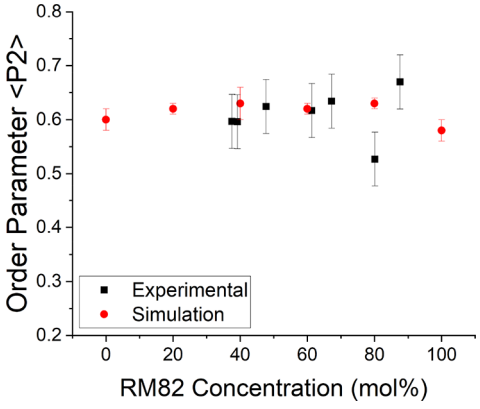

Figure 7. Order parameter of the nLCE systems plotted as a function of RM82 concentration showing agreement between MD simulation and experimental Raman spectroscopy.

For simulated LCE systems, the second-rank orientational order parameter, $\langle P_2 \rangle$, as a function of simulation time are given in the Supporting Information (Figure S1) with the average post-polymerization $\langle P_2 \rangle$ values plotted in Figure 7.

The order parameter calculated from MD simulations also demonstrates a near constant value, with an average of (0.61 ± 0.01), as a function of composition. This shows excellent agreement with experimental results (Figure 7) with average

https://doi.org/10.1021/acs.macromol.2c00587
Macromolecules XXXX, XXX, XXX−XXX

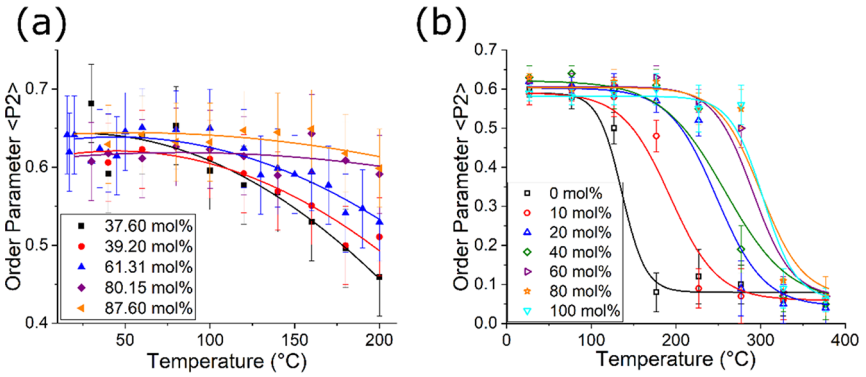

Figure 8. (a) Raman spectroscopy and (b) MD simulation temperature dependence of nematic LCE order parameter. Note the different scales of (a) and (b) reflecting the potential to take simulations to higher temperatures than experimentally available. Fitted curves are guides for the eye with fitting details in Tables S4 and S5.

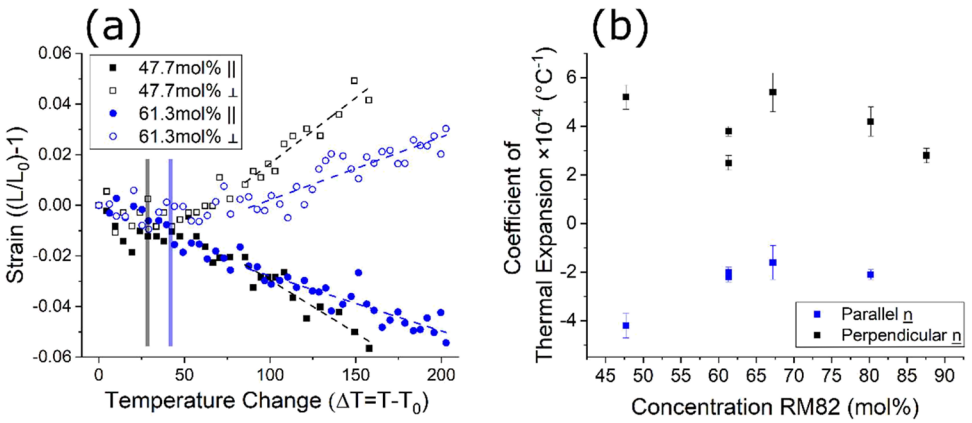

Figure 9. (a) Strain response as a function of temperature change for varying RM82 mol % nLCEs. Solid lines mark T_g for each sample. (b) Dependence of the CTE on the crosslinker concentration parallel and perpendicular to the director.

values being within error of one another. The near constant value of order parameter across compositions is expected as all monomer mixtures for nLCE fabrication/simulation are held at similar reduced temperatures (T-T_{NI}) during polymerization and thus should have comparable order parameters post-polymerization.

$\langle P_2 \rangle$ Temperature Dependence. The temperature dependence of $\langle P_2 \rangle$ for different composition nLCEs is experimentally measured from 30 to 200 °C using Raman spectroscopy. The temperature range is limited to 200 °C to avoid sample degradation. The temperature dependence of $\langle P_2 \rangle$ for varying RM82 concentrations is shown in Figure 8a for concentrations varying from 37.6 to 87.6 mol % RM82. It can be seen that there is a reduced temperature dependence in $\langle P_2 \rangle$ with increasing crosslinker concentration in the observable temperature range. It is noted that for the temperature and composition range experimentally observable, the LCE T_{NI} is not observed.

The temperature dependence of $\langle P_2 \rangle$ for post-reaction MD simulations was calculated for nLCEs with varying composition, 0 to 100 mol % RM82 (Figure 8b), at a range of temperatures from 30 to −380 °C.

It is found in MD simulations that the 0 mol % RM82 system (100 mol % A6OCB), of which an experimental thin-film sample cannot be fabricated, displays the strongest $\langle P_2 \rangle$ temperature dependence, demonstrating a clear nematic to isotropic phase transition at ∼150 °C, slightly higher than the experimentally observed T_{NI} for polymeric A6OCB of (122.6 ± 0.5) °C. The observed transition is slightly higher in MD simulation due to the finite simulation size. However, the ability to go to higher temperatures than experimentally available gives insight into the underlying trend in polymeric T_{NI}. Upon increasing the crosslinker concentration, the apparent nematic to isotropic transition temperature for the polymerized LCE increases, likely a result of an increase in the crosslinker density locking in the orientational order of the system to a greater extent. This compares well with experimental data. The temperature dependence of the measured $\langle P_2 \rangle$, at less than 200 °C, is observed to be greater for the samples with a lower crosslinker concentration and, by association, lower T_{NI}. For simulations that feature 60−100 mol % RM82, the nematic to isotropic transition occurs within the same temperature range (300−350 °C).

These combined results suggest that increasing the mesogenic crosslinker concentration causes not only an overall increase in T_g but also an increase in the LCE T_{NI}. For nLCEs with a high degree of crosslinking, T_{NI} is unobservable below the thermal decomposition temperature and as such cannot be experimentally verified. This dependence of LCE T_{NI} on composition will impact the thermo-mechanical response of the material, with the anisotropic shape change relating directly to changes in order parameter.[34]

LCE Thermo-macroscopic Response. The CTE of LCEs is anisotropic, depending on which axis is measured with respect to the nematic director. An increase in temperature for the LCE reduces the order parameter and thus, for prolate

https://doi.org/10.1021/acs.macromol.2c00587
Macromolecules XXXX, XXX, XXX−XXX

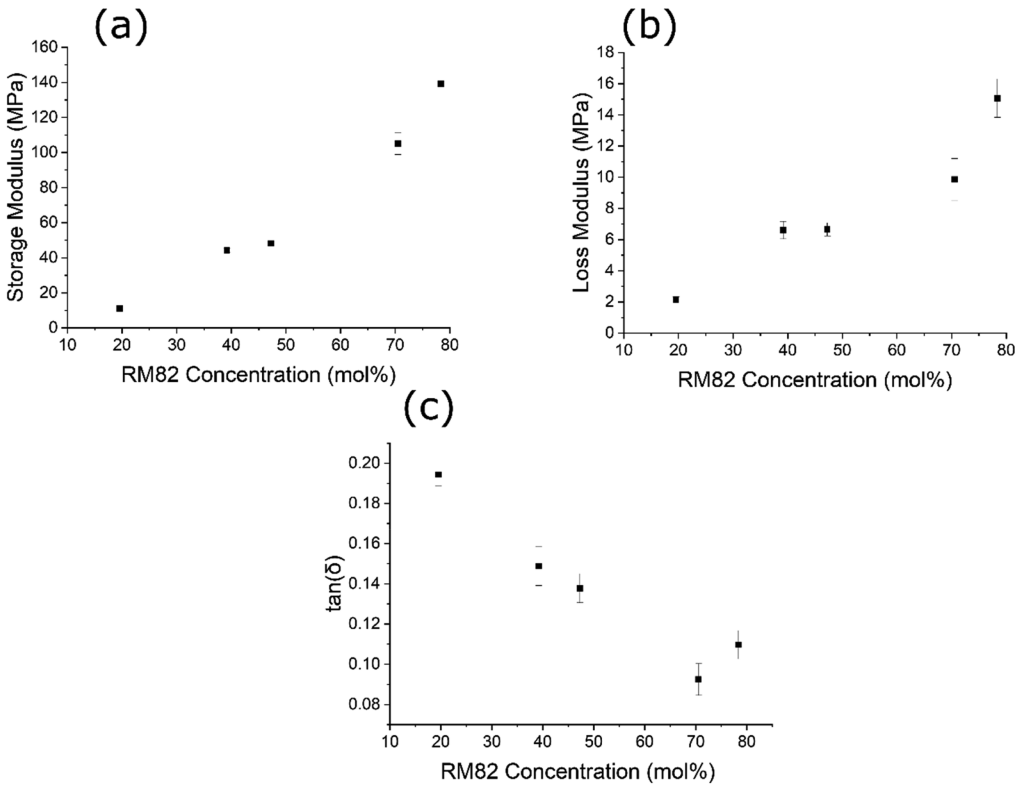

Figure 10. (a) Storage modulus, (b) loss modulus, and (c) tan(δ) dependence on RM82 crosslinker concentration for iLCEs. All measurements were taken 30 °C above T_g for each sample identified *via* DSC.

conformations (director and backbone align), reduces the elongation (ellipse) of the polymer backbone random walk. This in turn results in a macroscopic contraction along the director axis and an expansion along the perpendicular axis. The most notable shape change is when the LCE sample transitions through T_{NI},[34] though for these materials, T_{NI} is much greater than the degradation temperature of these samples, as established through DSC, Raman spectroscopy, and MD simulations.

This anisotropy in the CTE for LCEs is the underlying mechanism behind many proposed LCE actuator applications,[2−4] and therefore the tunability of this property is useful in the design of LCE materials. The macroscopic length (L) parallel (∥) and perpendicular (⊥) to the director is measured as a function of temperature (T) for nLCEs with varying RM82 concentration at >40 mol %. The strain, $\sigma = \frac{L}{L_0} - 1$, is plotted as a function of temperature change $\Delta T = T - T_0$, where L_0 is the initial length at a beginning temperature T_0, as shown in Figure 9a. The strain is directly related to the temperature change *via* the CTE ($\alpha_{\parallel,\perp}$). In most LCE studies of macroscopic shape change, the change in shape is plotted as a ratio of the current length to the isotropic length, which is not possible for the systems under investigation here due to their high nematic to isotropic transition temperatures.

The sample does not demonstrate a measurable shape change below the glass transition temperature. This is expected as the order parameter and polymer backbone are effectively locked while in the glassy polymeric state. Once the temperature exceeds T_g the order parameter begins to decrease and the associated anisotropic shape change can be observed, with a decreasing strain parallel to the director and an increasing strain perpendicular. To quantify the impact of LCE composition (RM82 concentration) on the anisotropic CTE of the LCEs, a linear fit was made at $\Delta T > 85$ °C, avoiding effects due to proximity to T_g. The gradient of the linear fit gives the CTE for the material, and Figure 9b shows the dependence of CTE parallel and perpendicular to the director on the RM82 concentration. A small but systematic reduction in the magnitude of CTE is seen with the increasing RM82 concentration. This would be expected for such a family of rubbers; the Simha−Boyer rule[35,36] states that the CTE ∼ $0.193/T_g$. Figure 4 shows an increase in T_g of ∼0.5 K/mol % RM82, so one would expect a reduction in the CTE from ∼5.8 × 10^{-4}/K at 47% RM82 to ∼5.3 × 10^{-4}/K at 87% RM82. Clearly, a much stronger variation is seen in Figure 9b, which can be attributed to the change in order. The increased T_{NI} with the increasing crosslinker concentration generates a reduced temperature dependence of order parameter in the measured range (<200 °C), in agreement with MD simulations and experimental Raman spectroscopy analysis (Figure 8). The closer the LCE is to T_{NI}, the greater the order parameter change with temperature and as such the greater the anisotropic shape change. As such, increasing the crosslinker concentration shifts T_{NI} to higher temperatures, lowering the observable dependence of CTE on temperature.

Control of LCE CTE is of crucial importance when designing materials for specific application in which the thermally induced anisotropic shape change is utilized, or where it needs to be avoided. Here, we have demonstrated that the anisotropy in CTE can be tuned in a controllable manner through composition variation and is largely a result of the modification to LCE T_{NI}.

LCE Mechanical Response. The LCE system presented here allows for a large variation in chemical composition while still allowing advantageous processing properties such as

https://doi.org/10.1021/acs.macromol.2c00587
Macromolecules XXXX, XXX, XXX−XXX

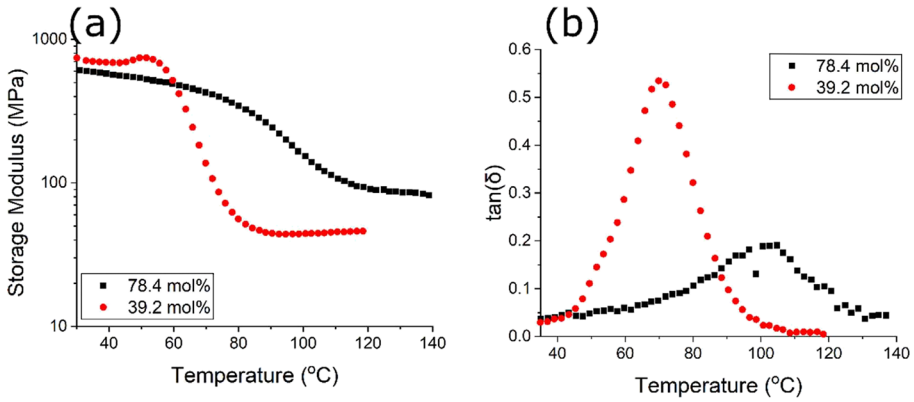

Figure 11. Temperature dependence of (a) storage modulus and (b) tan(δ) for 39.2 and 78.4 mol % RM82 iLCE samples.

monomer mixtures that exhibit a room temperature nematic phase and the ability for chemically identical materials with either nematic or isotropic ordering locked in during polymerization.[18] The variation of the ratio of the crosslinking moiety (RM82) to the monofunctional sidechain moiety (A6OCB) in this family of materials would be expected to also induce a large variation in the elastomers' mechanical properties. The mechanical properties of the nLCEs are anisotropic and depend strongly on whether the samples are monodomain or polydomain. Therefore, DMA was utilized to investigate the effect of crosslinker density on the mechanical properties of the iLCE systems, allowing us to understand the range of accessible storages and loss moduli in this family of materials. DMA experiments were performed on the iLCEs at a fixed temperature 30 °C above T_g (determined *via* DSC). The dependence of storage and loss moduli, together with tan(δ), is shown in Figure 10 as a function of crosslinker concentration for the iLCE samples.

Increasing the crosslinker concentration increases the measured storage modulus, an observation that agrees with similar trends observed in the rubbery plateau of poly(meth)-acrylate crosslinked systems.[37−39] Both the storage modulus, E', and the loss modulus, E'', (Figure 10a,b, respectively) increase approximately linearly on changing the crosslinker concentration from 19.5 to 78.4 mol %. The storage modulus varies from 11 to 140 MPa, while the loss ranges from 2.1 to 15 MPa. Thus, within the limits of available crosslinker concentrations where a homogeneous LCE can be fabricated, there is a factor of 12 variation in E' demonstrating the high tunability of this system. It is noteworthy that the storage modulus is high compared to other LCEs, a factor attributable to the relatively high crosslink density in these systems. While both the storage modulus and the loss modulus increase approximately linearly with the increasing crosslinker concentration, the storage modulus increases ca. 10% more rapidly than the loss modulus. This is reflected in the tan(δ) trend, Figure 8c, which decreases with increasing RM82 mol %. The increase in crosslinker density can also be considered as a direct decrease in the side-pendant unit, A6OCB. This dependence of tan(δ) on a reduced number of pendant groups is similar to trends observed in the non-liquid crystalline siloxane elastomer,[40] where a reduction in the concentration of a dangling pendant chains increased E' and reduced tan(δ) when measured in the rubbery plateau. The damping behavior of the non-liquid crystalline silicone elastomer mainly occurs due to pendant chains as they are free to relax into new equilibrium states when a strain is applied.[40] We suggest that this is also the underlying mechanism behind the observed dependence of tan(δ) on RM82, i.e., that the pendant A6OCB concentration dominates tan(δ). Thus, for the iLCE system presented herein, tan(δ) is also a tunable property.

Figure 11 demonstrates the results of a DMA temperature sweep at 1 Hz on iLCE samples with 39.2 and 78.4 mol % RM82. Figure 11a shows the storage modulus as a function of temperature. T_g may be identified by the onset of the drop in the storage modulus and in that case is determined to be 63 and 89 °C for the 39.2 and 78.4 mol % RM82 samples, respectively. This is within 10 °C of the T_g determined *via* DSC for these samples, with agreement that is typical between these two experimental techniques.[41] Below each material's glass transition, E' is comparable for the elastomers (~800 MPa). A broadening of the glass transition is noted for the higher RM82 concentration sample, potentially explained by a decrease in homogeneity across the sample with higher crosslink densities.[39,40]

At temperatures above T_g, the rubbery plateau, E' is higher for the higher RM82 concentration sample (~100 MPa) than the lower (~500 MPa), in agreement with the findings for all samples shown in Figure 10a. Figure 11b demonstrates the dependence of tan(δ) on temperature for these samples. It can be seen that the maximum value of tan(δ) is significantly greater for the 39.2 mol % sample than the 78.4 mol % sample, with peak amplitudes of 0.55 and 0.2, respectively. This is again in agreement with the trend seen in samples held at a constant temperature above T_g in Figure 10c. The higher concentration of pendant chains (lower crosslinker concentration) clearly results in a higher value of the peak tan(δ) due to the increasing potential the pendant side groups have to relax into new equilibrium states.

CONCLUSIONS

This paper has described the properties of a family of acrylate liquid crystal elastomers, designed for high tunability. The materials were synthesized in the laboratory and templated in both nematic and isotropic phases. Fully atomistic reactive molecular dynamics simulations were also used to generate polymer networks with templated isotropic/nematic order, the compositions of which closely approximates those studied experimentally in this paper. The simulations allowed various important polymer characteristics to be evaluated, including T_g, T_{NI}, and the order parameter $\langle P_2 \rangle$ and its dependence on temperature. The values deduced showed excellent agreement

https://doi.org/10.1021/acs.macromol.2c00587
Macromolecules XXXX, XXX, XXX−XXX

with the analogous LCEs synthesized in the laboratory. The *in silico* approach to polymerization that we describe in this paper therefore represents a new methodology to the design of liquid crystal elastomers.

It was noted both experimentally and in simulations that the glass transition temperatures of the members of this family of acrylates were systematically higher for the isotropic templated version (iLCE) than those templated in the nematic phase. The simulations allowed a deep insight into the reason for this observation: a higher conversion of the polymer in the iLCE than the equivalent nLCE system.

There was very good agreement between the experimentally determined value of the order parameter and the values deduced from simulation. The coefficient of thermal expansion of the LCEs was seen to be larger in systems where there was a larger degree of variation in $\langle P_2 \rangle$ over the temperature range explored, confirming the desirability of a relatively low T_{NI} in polymers designed for thermal shape actuation.

The acrylates described have a very high degree of tunability in their mechanical properties. There have been previous reports on the effect of varying chemical composition on the mechanical properties of LCEs.[42−44] Merkel *et al.* studied the effect of varying the concentration of the main-chain liquid crystal unit, RM257, while keeping the crosslink density constant, finding little difference in the storage modulus of the nematic rubbery plateau and isotropic rubbery plateau.[42] Saed *et al.* investigated the effect of crosslink density and functionality on a thiol-acrylate main-chain LCE system.[43] Tri-thiol and tetra-thiol crosslinkers were used in concentrations varying from 10 mol % to 80 mol %. It was shown that T_g increased by 12 and 22 °C with the increasing concentration of tri-thiol (5 to 17 °C) and tetra-thiol (3 to 25 °C) crosslinkers, respectively. The storage modulus, in the isotropic rubbery plateau, increased by a factor of ca. 2.3 with the increasing concentration of tri-thiol (0.9 to 2.1 MPa) and tetra-thiol (1.4 to 3.2 MPa) crosslinkers. The two-component acrylate chemical composition presented herein demonstrates a variation in the range of T_g of ca. 50 °C depending on the mol % RM82 and a 12× increase in E', thus demonstrating the high tunability of this system. The large variability in T_g and E' may be due to two reasons: (a) a reduction in crosslinker units is achieved by a replacement with the side-chain pendant unit A6OCB, which may contribute to mechanical properties[40] and (b) the use of the mesogenic crosslinker RM82. In any case, a clear dependence of T_g, storage modulus, loss modulus, and tan(δ) are seen with modification of the material composition. The dependence, in the rubbery plateau, of the storage modulus, the loss modulus, and tan(δ), is roughly linear, which demonstrates the ability to tailor these materials. One could predict, with relative ease, the behavior of a sample by simply taking a linear fit of the data shown.

■ ASSOCIATED CONTENT

Supporting Information

The Supporting Information is available free of charge at https://pubs.acs.org/doi/10.1021/acs.macromol.2c00587. The data associated with this paper is available from University of Leeds at https://doi.org/10.5518/1162.

Validation of the General Amber Force Field employed in this work; DSC of A6OCB; comment on MD simulation of conversion percentage; and fitting parameters for order parameter dependence on temperature (PDF)

■ AUTHOR INFORMATION

Corresponding Author

Helen F. Gleeson − *School of Physics and Astronomy, University of Leeds, Leeds LS2 9JT, U.K.;* orcid.org/0000-0002-7494-2100; Email: h.f.gleeson@leeds.ac.uk

Authors

Ethan I. L. Jull − *School of Physics and Astronomy, University of Leeds, Leeds LS2 9JT, U.K.;* Present Address: Present address: Debye Institute for Nanomaterials Science, Soft Condensed Matter and Biophysics, Utrecht University, 3508 TC Utrecht, The Netherlands (E.I.L.J.)

Richard J. Mandle − *School of Physics and Astronomy, University of Leeds, Leeds LS2 9JT, U.K.*

Thomas Raistrick − *School of Physics and Astronomy, University of Leeds, Leeds LS2 9JT, U.K.;* orcid.org/0000-0002-6227-6550

Zhaopeng Zhang − *School of Physics and Astronomy, University of Leeds, Leeds LS2 9JT, U.K.*

Peter J. Hine − *School of Physics and Astronomy, University of Leeds, Leeds LS2 9JT, U.K.*

Complete contact information is available at: https://pubs.acs.org/10.1021/acs.macromol.2c00587

Funding

The authors are grateful for funding from the Northern Triangle Initiative. T.R. acknowledges funding from the University of Leeds Alumni fund.

Notes

The authors declare no competing financial interest.

■ ABBREVIATIONS

LCE, liquid crystal elastomer; LC, liquid crystal; nLCE, nematic liquid crystal elastomer; iLCE, isotropic liquid crystal elastomer; MD, molecular dynamics; GAFF, General Amber Force Field; NVE, constant volume, constant energy; NVT, constant temperature, constant volume; NPT, constant temperature, constant pressure; $\langle P_2 \rangle$, order parameter; T_g, glass transition temperature; T_{NI}, nematic to isotropic transition temperature; T_{KN}, crystal to nematic transition temperature; CTE, coefficient of thermal expansion; RM82, 1,4-bis-[4-(6-acryloyloxyhexyloxy)benzoyloxy]-2-methylbenzene; A6OCB, 4-[(6-acryloyloxy)hexyloxy]-4′-cyanobiphenyl; DSC, differential scanning calorimetry; DMA, dynamic mechanical analysis; E', storage modulus; E'', loss modulus; p%, degree of polymerization

■ REFERENCES

(1) Andrienko, D. Introduction to liquid crystals. *J. Mol. Liq.* **2018**, *267*, 520−541.

(2) Ula, S. W.; Traugutt, N. A.; Volpe, R. H.; Patel, R. R.; Yu, K.; Yakacki, C. M. Liquid crystal elastomer: an introduction and review of emerging technologies. *Liq. Cryst. Rev.* **2018**, *6*, 78−107.

(3) Thomsen, D. L., III; Keller, P.; Naciri, J.; Pink, R.; Jeon, H.; Shenoy, D.; Ratna, B. R. Liquid crystal elastomers with mechanical properties of a muscle. *Macromolecules* **2001**, *34*, 5868−5875.

(4) Buguin, A.; Li, M.; Silberzan, P.; Ladoux, B.; Keller, P. Micro-actuators: When artificial muscles made of nematic liquid crystal elastomers meet soft lithography. *J. Am. Chem. Soc.* **2006**, *128*, 1088−1089.

(5) Li, M.; Keller, P. Artificial muscles based on liquid crystal elastomers. *Phil. Trans. R. Soc. A* **2006**, *364*, 2763−2777.
(6) Luo, C.; Chung, C.; Traugutt, N. A.; Yakacki, C. M.; Long, K. N.; Yu, K. 3D printing of liquid crystal elastomer foams for enhanced energy dissipation under mechanical insult. *Appl. Mater. Interfaces* **2021**, *13*, 12698−12708.
(7) Traugutt, N. A.; Mistry, D.; Luo, C.; Yu, K.; Ge, Q.; Yakacki, C. M. Liquid-crystal-elastomer-based dissipative structures by digital light processing 3d printing. *Adv. Mater.* **2020**, *32*, 2000797.
(8) Clarke, S. M.; Tajbakhsh, A. R.; Terentjev, E. M.; Remillat, C.; Tomlinson, G. R.; House, J. R. Soft elasticity and mechanical damping in liquid crystalline elastomers. *J. Appl. Phys.* **2001**, *89*, 6530−6535.
(9) Zhang, Y.; Wang, Z.; Yang, Y.; Chen, Q.; Qian, X.; Wu, Y.; Liang, H.; Xu, Y.; Wei, Y.; Ji, Y. Seamless multimaterial 3D liquid-crystalline elastomer actuators for next-generation entirely soft robotics. *Sci. Adv.* **2020**, *6*, No. eaay8606.
(10) Mistry, D.; Gleeson, H. F. Mechanical deformations of a liquid crystal elastomer at director angles between 0° and 90°: Deducing an empirical model encompassing anisotropic nonlinearity. *J. Polym. Sci., Part B: Polym. Phys.* **2019**, *57*, 1367−1377.
(11) Sánchez-Ferrer, A.; Finkelmann, H. Thermal and mechanical properties of new main-chain liquid-crystalline elastomers. *Solid State Sci.* **2010**, *12*, 1849−1852.
(12) Mani, S. A.; Hadkar, S. U.; Jessy, P. J.; Lal, S.; Keller, P.; Khosla, S.; Sood, N.; Sarawade, P. Study of the optical, thermal, and mechanical properties of nematic liquid crystal elastomers. *J. Inf. Disp.* **2016**, *17*, 169−176.
(13) Brannum, M. T.; Steele, A. M.; Venetos, M. C.; Korley, L. T. J.; Wnek, G. E.; White, T. J. Light control with liquid crystalline elastomers. *Adv. Opt. Mater.* **2019**, *7*, 10801683.
(14) Traugutt, N. A.; Volpe, R. H.; Bollinger, M. S.; Saed, M. O.; Torbati, A. H.; Yu, K.; Dadivanyan, N.; Yakacki, C. M. Liquid-crystal order during synthesis affects main-chain liquid-crystal elastomer behavior. *Soft Matter* **2017**, *13*, 7013−7025.
(15) Boothby, J. M.; Volkenburg, T. V.; Le, N. Q.; Ohiri, K.; Hagedon, M.; Xia, Z. Effects of network structure on the mechanical and thermal responses of liquid crystal elastomers. *Multi. Mater.* **2020**, *3*, No. 0.15002.
(16) Spillmann, C. M.; Nacir, J.; Chen, M.; Srinivasan, A.; Ratna, B. R. Tuning the physical properties of a nematic liquid crystal elastomer actuator. *Liq. Cryst.* **2006**, *33*, 373−380.
(17) Jia, Y.; Zhang, B.; Zhou, E.; Feng, Z.; Zang, B. Synthesis and characterization of network liquid crystal elastomers and thermosets. *J. Appl. Polym. Sci.* **2002**, *85*, 1104−1109.
(18) Mistry, D.; Nikkhou, M.; Raistrick, T.; Hussain, M.; Jull, E. I. L.; Baker, D. L.; Gleeson, H. F. Isotropic liquid crystal elastomers as exceptional photoelastic strain sensors. *Macromolecules* **2020**, *53*, 3709−3718.
(19) Plimpton, S. Fast parallel algorithms for short-range molecular dynamics. *J. Comput. Phys.* **1995**, *117*, 1−19.
(20) Wang, J.; Wolf, R. M.; Caldwell, J. W.; Kollman, P. A.; Case, D. A. Development and testing of a general amber force field. *J. Comput. Chem.* **2004**, *25*, 1157−1174.
(21) Martínez, L.; Andrade, R.; Birgin, E. G.; Martínez, J. M. Packmol: A package for building initial configurations for molecular dynamics simulations. *J. Comput. Chem.* **2009**, *30*, 2157−2164.
(22) Gissinger, J. R.; Jensen, B. D.; Wise, K. E. Modeling chemical reactions in classical molecular dynamics simulations. *Polymer* **2017**, *128*, 211−217.
(23) Gissinger, J. R.; Jensen, B. D.; Wise, K. E. Reacter: A heuristic method for reactive molecular dynamics. *Macromolecules* **2020**, *53*, 9953−9961.
(24) McGibbon, R. T.; Beauchamp, K. A.; Harrigan, M. P.; Klein, C.; Swails, J. M.; Hernández, C. X.; Schwantes, C. R.; Wang, L. -P.; Lane, T. J.; Pande, V. S. Mdtraj: A modern open library for the analysis of molecular dynamics trajectories. *Biophys. J.* **2015**, *109*, 1528−1532.
(25) Humphrey, W.; Dalke, A.; Schulten, K. Vmd: Visual molecular dynamics. *J. Mol. Graph* **1996**, *14*, 33−38.
(26) Hohne, G. W. H.; Gemminger, W. F.; Flammersheim, H. J. *Differential Scanning Calorimetry Second Edition*; Springer-Verlag, 2003
(27) Raistrick, T.; Zhang, Z.; Mistry, D.; Mattsson, J.; Gleeson, H. F. Understanding the physics of the auxetic response in a liquid crystal elastomer. *Phys. Rev. Res.* **2021**, *3*, No. 023191.
(28) Southern, C. D.; Gleeson, H. F. Using the full Raman depolarisation in the determination of the order parameters in liquid crystal systems. *Eur. Phys. J. E: Soft Matter Biol. Phys.* **2007**, *24*, 119−127.
(29) Hsu, E. C. H.; Johnson, J. F. Phase diagrams of binary nematic mesophase systems. *Mol. Cryst. Liq. Cryst.* **1973**, *20*, 177−190.
(30) Hulme, D. S.; Raynes, E. P.; Harrison, K. J. Eutectic mixtures of nematic 4′-substituted 4-Cyanobiphenyls. *J. Chem. Soc., Chem. Commun.* **1974**, *1549*, 98−99.
(31) Zhang, B.-Y.; Liu, L.-M.; Yao, D.-S.; Zhang, L.-F. Phase behavior of liquid crystalline elastomers based on a tri-vinyl mesogenic cross-linker. *Colloid Polym. Sci.* **2005**, *283*, 1143−1148.
(32) Dvinskikh, S. V.; Furó, I.; Zimmermann, H.; Maliniak, A. Ansitropic self-diffusion in thermotropic liquid crystals studied by ^{1}H and ^{2}H pulse-field-gradient spin-echo NMR. *Phys. Rev., E* **2002**, *65*, No. 061701.
(33) Kamal, T.; Park, S. Y. Shape-responsive actuator from a single layer of a liquid-crystal polymer. *ACS Appl. Mater. Interfaces* **2014**, *6*, 18048−18054.
(34) Finkelmann, H.; Greve, A.; Warner, M. The elastic anisotropy of nematic elastomers. *Eur. J. Phys. E* **2001**, *5*, 281−293.
(35) Simha, R.; Boyer, R. F. On a general relation involving the glass temperature and coefficients of expansion of polymers. *J. Chem. Phys.* **1962**, *37*, 1003−1007.
(36) Mark, J. E. *Physical Properties of Polymers Handbook,* Springer:, New York, 2007, DOI: 10.1007/978-0-387-69002-5
(37) Ortega, A. M.; Kasprzak, S. E.; Yakacki, C. M.; Diani, J.; Greenberg, A. R.; Gall, K. Structure-Property relationships in photopolymerizable polymer networks: effect of composition on the crosslinked structure and resulting thermomechanical properties of a (Meth)acrylate-based system. *J. Appl. Polym. Sci.* **2008**, *110*, 1559−1572.
(38) Safranski, D. L.; Gall, K. Effect of chemical structure and crosslinking density on the thermo-mechanical properties and toughness of (meth)acrylate shape memory polymer networks. *Polymer* **2008**, *49*, 4446−4455.
(39) Kannurpatti, A. R.; Anseth, J. W.; Bowman, C. N. A study of the evolution of mechanical properties and structural heterogeneity of polymer networks formed by photopolymerizations of multifunctional (meth)acrylates. *Polymer* **1998**, *39*, 2507−2513.
(40) Urayama, K.; Miki, T.; Takigawa, T.; Kohjiya, S. Damping elastomer based on model irregular networks of end-linked Poly-(Dimethylsiloxane). *Chem. Mater.* **2004**, *16*, 173−178.
(41) Achorn, P. J.; Ferrillo, R. G. Comparison of thermal techniques for glass transition measurements of polystyrene and cross-linked acrylic polyurethane films. *J. Appl. Polym. Sci.* **1994**, *54*, 2033−20423.
(42) Merkel, D. R.; Traugutt, N. A.; Visvanathan, R.; Yakacki, C. M.; Frick, C. P. Thermomechanical properties of monodomain nematic main-chain liquid crystal elastomers. *Soft Matter* **2018**, *14*, 6024−6036.
(43) Saed, M. O.; Torbati, A. H.; Starr, C. A.; Visvanathan, R.; Clark, N. A.; Yakacki, C. M. Thiol-acrylate main-chain liquid-crystalline elastomers with tunable thermomechanical properties and actuation strain. *J. Polym. Sci., Part B: Polym. Phys.* **2017**, *55*, 157−168.
(44) Hotta, A.; Terentjev, E. M. Dynamic soft elasticity in monodomain nematic elastomers. *Eur. Phys. J. E* **2003**, *10*, 291−301.

https://doi.org/10.1021/acs.macromol.2c00587
Macromolecules XXXX, XXX, XXX−XXX